

Underwater Acoustic Physical Layer Emulator to Evaluate Digital Communications

M.S. Martins^{ab}, J. Cabral^a.

^aCMEMS, University of Minho
Campus of Azurém, Guimarães, Portugal

^bLARSyS, University of Algarve
Campus de Gambelas, PT-8005-139 Faro, Portugal
email: mmartins@dei.uminho.pt
cabral@dei.uminho.pt

G. Lopes^c, F. Ribeiro^c.

^cAlgoritmi Center, University of Minho, Campus of
Azurém, Guimarães, Portugal
email: gil@dei.uminho.pt
fernando@dei.uminho.pt

Abstract—In order to achieve underwater acoustic high data-rate and real time communications, it is essential to implement a system that operates both at high and wideband frequencies using digital modulations. Therefore, to reduce the time and cost of developing acoustic communications an emulator of a physical layer model was implemented, allowing to test in real time the performance of digital modulations. The model was composed of an emitter transducer, a hydrophone and the subaquatic medium and was integrated in a Field Programmable Gate Array (FPGA) in order to emulate the physical layer in the acoustic modem testing. The emitter transducer and the hydrophone models were designed to meet real prototype characteristics. The system prototype was implemented in order to compare the experimental trials results with those obtained in emulator, emulating the transmission of acoustic signals, using different types of digital modulations. The system was tested using Binary Phase-Shift Keying (BPSK), Binary Frequency Shift keying (BFSK) and Binary Amplitude Shift Keying (BASK) modulations with a 1 MHz carrier frequency resulting in a data rate of 125 kbps. It was verified that the implemented model represents a suitable approximation to the real subaquatic communication channel, allowing the evaluation of digital acoustic communications.

Keywords—Underwater Digital Communications; Acoustic Transducer Simulation; Acoustic Communications Emulator.

I. INTRODUCTION

Underwater wireless communications are a decisive technology for underwater sensor networks, divers and submarine communications, robotics and Autonomous Underwater Vehicle (AUVs) navigation and control.

Therefore, it is imperative to find reliable solutions, able to fulfill all these needs. There are three main forms to communicate through water: acoustic, radio frequency and optical [1]. Radio frequency is limited by the high level of absorption in water [2]. Optical systems suffer from the same limitation as well as the disadvantages associated to the high levels of ambient light close to the water surface and scattering due to suspended particles [3]. As a result, acoustic communication systems are the preferential form of wireless underwater communications, since they show low sound attenuation in water [4]. Acoustic communications have been used for long distance communications, up to 20 km, and in deep waters with stable thermal conditions. But, despite underwater wireless communications having shown

strong advances in recent years, there are still many limitations concerning data rates and robustness for real-time applications [5].

There are several solutions to increase the modulation efficiency or data rate. The most used solutions are: increasing the carrier frequency [6] or increasing the symbol rate per carrier period [7].

High frequencies also raise strong problems related to attenuation. Being directly related to the frequency, the acoustic absorption at 1 MHz can reach 280 dB/km [13]. Consequently, the maximum communication range decreases dramatically to a few hundred meters or less with the increasing of frequency [8]. On the other hand, real time acoustic communications are not supported at long distances, since acoustic waves propagate at around 1500 m/s, resulting in high propagation delays and disabling, therefore, any real time connection [8]. Therefore, high data rate transmissions are only reliable for short and medium distances.

There are works showing that it is possible to use frequencies up to 1 MHz to achieve high data rate acoustic communications. For example, in [9] the authors presented an acoustic FPGA based on a modem operating at frequencies between 100 kHz and 1 MHz, for distances ranging between 50 m and 100 m. Using a BPSK modulation with a 800 kHz carrier frequency, the system archived a 80 kbps data rate.

In the previous work the authors presented an underwater low power acoustic modem to operate over tens of meters, achieving a maximum data rate of 1 Mbps using carriers up to 1 MHz [10] [11].

However, the development of acoustic technology for underwater applications consumes high amounts of time and resources. Therefore, the proposed emulator allows a rapid development and test of acoustic modems. Allowing in the test digital modulations performance before implementing in a field, helping in the selection the most reliable solutions reducing the development time and cost. To do so, it was necessary to implement a communication system composed by an emitter transducer, a hydrophone and the corresponding conditioning electronics to experimentally validate the emulator results. The underwater channel model was implemented and tested in shallow waters, including MHz frequency range, directional spreading type, attenuation, ambient noise, Doppler Effect, propagation delay and multipath. To complete the system it was necessary to implement a model for piezoelectric

transducers. The selected emitter was a homemade Piston type transducer for a directional beam. The hydrophone was a commercial transducer Cetacean Research™ C304XR with linear response ($\pm 3\text{dB}$) for a frequency range between 0.012 and 1000 kHz [12].

In Section 2, a small physical properties background of the underwater acoustic channel and ultrasonic transducer is introduced. In Section 3, the experimental setup is presented and, in Section 4, the physical layer emulator implementation is described. Section 5, present the results of the emulator model evaluation and the comparisons with real trials. Finally, in Section 6, conclusions and future work are presented.

II. PHYSICAL LAYER BACKGROUND

The underwater acoustic communication physical layer is composed by the emitter ultrasonic transducer, hydrophone and the subaquatic medium. To allow a better understanding of the underwater acoustics, this section will present the physics background of the ultrasonic transducer and subaquatic medium.

A. Underwater Acoustic Channel

Despite the advantages of acoustic communication in underwater environments, when compared to optical and radio, the propagation of sound also has significant challenges that influence the development of underwater acoustic communication systems. This is mainly due to the slow speed of acoustic propagation in water (about 1500 m/s). When studying sound propagation in the underwater acoustic channel, some relevant phenomena must be taken into account: attenuation, ambient noise, Doppler Effect, propagation delay and multipath [8].

B. Ultrasonic transducers

The ultrasonic transducers are commonly made using piezoelectric materials, because they present good response to high frequencies. The ultrasonic transducers convert the electric energy into sound and vice versa [13]. Therefore, to implement an ultrasonic transducer model it is necessary to comprehend piezoelectric material response and behavior. There are several factors that influence the transducer performance, namely the structural damping, acoustic impedance mismatch and electrical damping [14]. Structural damping is due to the energy dissipation and reaction time in the geometrical deformations of the transducer when the electrical field is applied. The acoustic impedance mismatch, between the transducer and the medium, causes acoustic waves to be reflected back to transducer. The resonance transducers are designed to overcome this fact, since the internal acoustic waves are synchronized with the electrical drive signal, causing an addition of the two signals and therefore increasing the output. Electrical damping is due to transducer capacitor effects which result in a time lag between the application of the electrical signal and the transducer response. However, this effect can be corrected by implement an impedance matching circuit, therefore this matter will not be addressed in this document.

Piezoelectric ultrasound transducers, at high frequencies, usually operate in the 33 mode, that is, the deformation along the polarization axis and the excitation electric field point into the same direction. Consequently, in this work, it will only be addressed the piston type transducer operating in thickness mode. The free displacement of the material in direction 3, without restraining force and assuming uniform strain over the surface [14], is given by:

$$\xi = nvd_{33} \quad (1)$$

where ξ is the free displacement, v is the applied voltage, d_{33} is the coupling coefficient in the thickness direction and n is the number of layers.

The displacement is also dependent on the stress and strain of the viscoelasticity of the piezoelectric material, resulting in a structural damping. When an electric field is applied to the polymer charged particles, they move inside the actuator to align the charges. In this process, some of the energy is dissipated and the reaction time is also affected. The final displacement for a piezoelectric stack transducer, operating in the 33 mode, can be written as a function of the nondimensional frequency [14]:

$$\frac{u(\sigma)}{u_{st}} = \frac{RC_p^S \omega_m \sigma + 1}{(\sigma^2 + 1)(RC_p^S \omega_m \sigma + 1) + k_{33}^2 RC_p^S \omega_m \sigma}, \quad \sigma = \frac{S}{\omega_m} \quad (2)$$

where σ is the nondimensional frequency in which 1 represents the short circuit mechanical resonance, R is the shunt resistance, C_p^S is the stain-free capacitance, ω_m is the short circuit mechanical resonance and k_{33}^2 is the generalized piezoelectric coupling coefficient. The ω_m and k_{33}^2 can be calculated with (3) and (4), respectively.

$$k_{33}^2 = 1 - S_{33}^E \epsilon_{33}^T \quad (3)$$

$$\omega_m = \frac{k + k_a^E}{m} \quad (4)$$

k is the viscoelastic stiffness, k_a^E is the short circuit stiffness of the actuator, m is the actuator mass and ϵ_{33}^T is the stress free dielectric permittivity.

Another important aspect is related to the transducer acoustic impedance. The sound wave created inside the transducer reflects, in part, at the boundary established by different densities and bulk modulus B of the transducers and the medium according to the Snell's law [15]. This reflection creates deformations on the acoustic signal transmitted to the medium [13], which can be calculated by:

$$a_{out}(t) = lt_w (a_{in}(t) + r_w a_{in}(t + D_p)) \quad (5)$$

Converting to the Laplace domain we obtain the following transfer function:

$$\frac{A_{out}(s)}{A_{in}(s)} = LT_w(1 + R_w e^{sD_p}) \quad (6)$$

Here, a_{out} is the sound wave output as function of time t , a_{in} is the sound wave as function of time created inside the active element, t_w is the transmitted sound wave intensity percentage, r_w is the reflected sound wave intensity percentage, l is the internal acoustic energy loss and D_p is the delay of the reflected sound wave, introduced by the active element thickness.

III. EXPERIMENTAL SETUP

In order to achieve high data-rate communications, it was essential to implement a system prototype that operates at high frequencies (up to 1 MHz). The acoustic system was designed to be reconfigurable and reprogrammable, over dimensioning all parts of the system allowing future upgrades.

A. Acoustic Modem

In order to design an acoustic modem capable of performing several types of digital modulations, a highly adaptable system was developed.

The acoustic modem was implemented in a Xilinx Spartan-3A, which is responsible for modulation and demodulation, control of the receiver instrumentation and output amplifiers. The system runs with an external clock of 50 MHz. The receiver is composed in this order by 100kHz High Pass Filter, which removes all the low frequency noises, a variable gain control amplifier, from -22 to 20 dB, a Antialiasing filter and an ADC AD9244. To driver signals at the output of the FPGA modulator a DAC DAC904 and a Class B Push-Pull symmetric voltage amplifier were implemented with a of 12 dB gain. The ultrasonic emitter was a homemade PZT-5H 2 mm piston type transducer with 2 cm diameter [16]. Despite the transducer's directionality, a residual pressure wave projected in the transducer rear can achieve 15% of the main front pressure wave amplitude. The ultrasonic receptor used to register the pressure waves was the Cetacean Research™ C304XR hydrophone, with a transducer sensibility of -201 dB, re 1 V/μPa and a linear Frequency Range (±3dB) of 0.012–1000 kHz. The filter block consists of a 2nd order band-pass filter from 0.001 to 2 MHz with a gain in the pass band of 6dB. The digital oscilloscope used to record the measurements was a PicoScope 4227 100 MHz.

IV. PHYSICAL LAYER EMULATION SYSTEM

The physical layer emulator allows testing the acoustic modem performance for different types of digital modulations without physical implementation. This process reduces the cost and time spent. The emulator consists in a computer model for all physical layers blocks to be integrated in the FPGA program. Therefore the FPGA, in addition to modulate and demodulate functions, still emulates the acoustic modem electronics and the subaquatic medium, as presented in Figure 1.

The modulator and demodulator were implemented according to the selected type of modulation: BPSK, BFSK and BASK. Since, the emulator model was implemented in a discrete algorithm (Z-Transform), it was not necessary to implement the analog to digital and digital to analog converters (ADC and DAC) blocks.

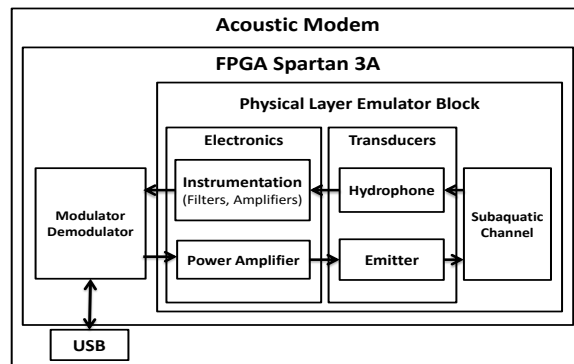


Figure 1. Physical layer emulation blocks.

The algorithm is divided in three parts: the electronics model, the transducer and channel model. The electronics model is a fixed model where is not necessary to define any variables, since electronics circuits model (instrumentation and power amplifier) were implemented using digital filters according to the correspondent transfer function available in each component datasheet. The transducer and the channel model are user defined models where is necessary to define the system variables such as: transducer characteristics (mechanical and electrical characteristic), medium characteristics (temperature, salinity, acidity, shipping factor and wind speed) and the scenario setup (dimensions, hydrophone position, emitter position, reference distance, hydrophone and emitter velocity relative to the medium).

V. RESULTS

This section shows the results obtained in the experimental tests in order to compare them with those obtained by the emulator.

The experimental analysis tested the attenuation, multipath and transducer response to digital modulations. The Doppler Effect and noise was discarded. This decision was justified by the great difficulty in assembling an experimental setup with moving parts in the medium and at 1 MHz the underwater environment is relatively silent.

A. Attenuation

The swimming pool was 12 m long, 4 m wide and 3 m deep. Four test distances were defined: 1, 4, 8 and 12 m, where measurements were performed at 50 cm deep and in the middle of the pool (2 m either side). At each distance, several frequencies were tested: 100 kHz, 200 kHz, 300 kHz, 400 kHz, 500 kHz, 600 kHz, 700 kHz, 800 kHz, 900 kHz, 1 MHz, 1.2 MHz and 1.4 MHz.

The simulation was configured with the conditions observed in the experimental tests, with fresh water at a temperature of 13 °C and 7.2 pH.

The projector and the hydrophone sound wave level responses are irrelevant since the considered results are relative. A reference measurement was taken at 10 cm intervals over several distances for all the tested frequencies and attenuation, and calculated according to the following equation:

$$20\log_{10}\left(\frac{p}{p_{ref}}\right) \quad (7)$$

where p is the value of the pressure wave at the receiver and the p_{ref} is the value of the pressure wave at the reference distance. The experimental values are presented as an average of 10 measurements, with a maximum error of 3.5%.

Figure 2 shows that attenuation increases with the increasing distance. The 1 MHz point shows a low attenuation peak in all the curves that gets smoother with the increasing distance. This fact is related to the emitter optimal frequency (resonance point). Moreover, attenuation does not increase with the increasing frequency as the beam divergence angle decreases with frequency.

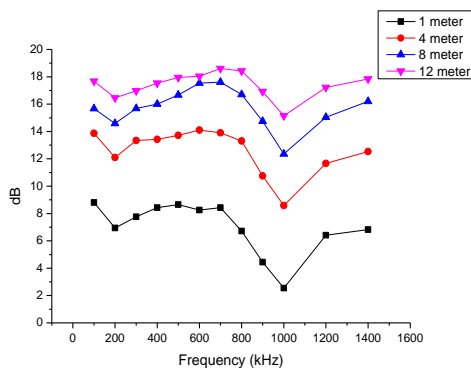


Figure 2. Experimental attenuation results as a function of frequency.

The simulation (Figure 3) shows the overall results with lower attenuations, but the general trend is similar to that obtained with the experimental results. The resemblance between the two curves increases with the increasing distance.

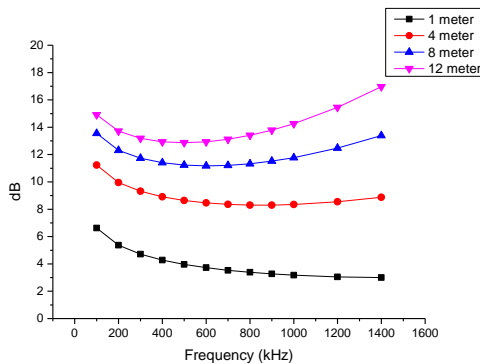


Figure 3. Emulator attenuation results as a function of frequency.

The difference between the experimental and the simulated results assumes an average of 3.2 dB reaching a 6

dB peak. This difference occurs because the used model was developed for a range of kilometers rather than meters and the low attenuation peak at 1 MHz in all the graphics is due to the transducer optimal operational frequency.

B. Multipath

The multipath performance was also evaluated in the pool where a burst signal of 20 cycles at 1 MHz, over a distance of 12 m was transmitted. The ultrasonic emitter and hydrophone positions were (0.03; 1.95; 0.5) and (11.61; 1.95; 0.5) meters. At this frequency, both the emitter and the hydrophone operate in a directional pattern.

Figure 4 shows the experimental results for the second configuration.

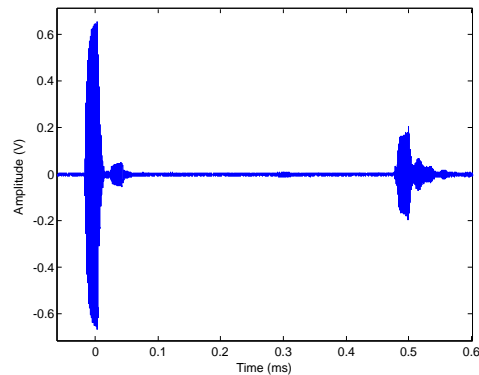


Figure 4. Multipath signal received from a burst signal of 20 cycles at 1 MHz over 12 meters.

Figure 4 also shows three sets of signals. At 1 MHz the transducer was operating in a directional pattern with a divergence angle of 4.3° and, therefore, only the back and front echoes appear in the results.

The first set is from the direct path, the second is from the back echo and the third is from the front echo. The back echo has lower amplitude than the front echo, despite traveling a shorter distance. This is due as the back echo results from a residual energy loss in the rear part of the transducer.

Figure 5 shows the emulation results for the second configuration.

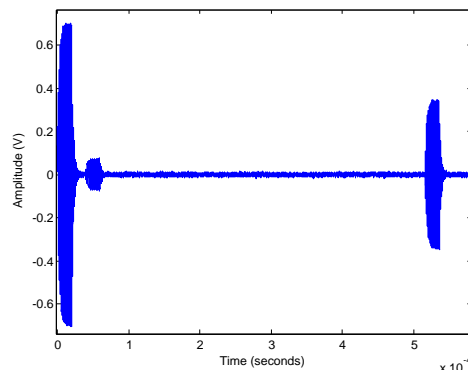


Figure 5. Multipath emulation of a burst signal of 20 cycles at 1 MHz over 12 meters.

The emulator achieves a good approximation to the real-world case, with similar phase and amplitude distortion, despite the simulation only including the 1st order echoes.

C. Transducers response to digital modulation

In order to evaluate the performance of ultrasound transducers, using digital modulations, fundamental modulations such as BPSK, BFSK and BASK were considered [17]. The carrier frequency was set to 1 MHz with a 125 kbps baud rate.

Figures 6, 7 and 8 show the transducer's behavior to the BPSK, BFSK and BASK modulations, respectively. Each figure shows the modulation signal, the FPGA emulation and the real test signal.

Figure 6c shows the BPSK modulation, where the 180° phase shift corresponds to the logic level transition. The PZT transducer shows a high damping effect due to the energy stored inside the transducer. In the moment of phase shift the two signals try to cancel one another.

In the BFSK drive signal of Figure 7 the high logic level '1' and the low logic level '0' were modulated with carriers of 1 MHz and 500 kHz, respectively. In the FSK modulation, the carrier frequencies are usually adopted with close values, but, in order to simplify the evaluation, the option of using two very distinct frequencies was taken. The 500 kHz frequency is highly attenuated due to two factors, the first is that the transducer acoustic output is proportional to the frequency, resulting in half amplitude and, the second is that the transducer was projected to operate at maximum optimization point at 1 MHz.

In the BASK, the low logic level was set to half of the high logic level amplitude, as presented in figure 8a. Similar to the BFSK test, the transducer shows also a high damping effect resulting in slow amplitude variations.

Comparing Figures 6b, 7b and 8b with the Figures 6c, 7c and 8c it is possible to observe the similarity between emulations and real tests, confirming the suitability of the developed model.

VI. CONCLUSIONS AND FUTURE WORK

A physical layer FPGA based emulator for underwater acoustic communications was developed. The model was designed specifically to emulate the acoustic channel and ultrasonic transducers, allowing performance evaluation for of the ultrasound communications using digital modulations.

The acoustic underwater communication channel model was taking into account several phenomena: attenuation, multipath, environment noise and propagation delay. Real tests were also implemented to validate the attenuation, multipath and propagation delay.

The transducer models, using digital modulations, were simulated and validated with real tests. The results show that the transducer models present a similar response to real tests.

Overall, the results show that the model represents a useful approximation to the real subaquatic communication channel, being therefore an important tool to simulate the propagation of acoustic signals.

In future works, we will implement and test a communication using Frequency Division Multiplexing (FDM) modulations in order to achieve data rates in the order of 1.5 to 2 Mbps.

ACKNOWLEDGMENT

M. S. Martins thanks the FCT for the Post-Doctoral fellowships grant SFRH/BPD/107826/2015.

REFERENCES

- [1] M. Chitre, S. Shahabudeen, and M. Stojanovic, "Underwater Acoustic Communications and Networking: Recent Advances and Future Challenges," *Mar. Technol. Soc. J.*, vol. 42, no. 1, pp. 103–116, Mar. 2008.
- [2] X. Che, I. Wells, G. Dickers, P. Kear, and X. Gong, "Re-evaluation of RF electromagnetic communication in underwater sensor networks," *IEEE Commun. Mag.*, vol. 48, no. 12, pp. 143–151, Dec. 2010.
- [3] G. Baiden, Y. Bissiri, and A. Masoti, "Paving the way for a future underwater omni-directional wireless optical communication systems," *Ocean Eng.*, vol. 36, no. 9–10, pp. 633–640, Jul. 2009.
- [4] I. F. Akyildiz, D. Pompili, and T. Melodia, "Underwater acoustic sensor networks: research challenges," *Ad Hoc Networks*, vol. 3, no. 3, pp. 257–279, May 2005.
- [5] S. Roy, T. M. Duman, V. McDonald, and J. G. Proakis, "High-Rate Communication for Underwater Acoustic Channels Using Multiple Transmitters and Space-Time Coding: Receiver Structures and Experimental Results," *IEEE J. Ocean. Eng.*, vol. 32, no. 3, pp. 663–688, Jul. 2007.
- [6] N. Nowsheen, C. Benson, and M. Frater, "Design of a high frequency FPGA acoustic modem for underwater communication," in *OCEANS'10 IEEE SYDNEY*, 2010, pp. 1–6.
- [7] J. Huang, S. Zhou, and Z. Wang, "Performance Results of Two Iterative Receivers for Distributed MIMO OFDM With Large Doppler Deviations," *IEEE J. Ocean. Eng.*, vol. 38, no. 2, pp. 347–357, Apr. 2013.
- [8] M. Stojanovic and J. Preisig, "Underwater acoustic communication channels: Propagation models and statistical characterization," *IEEE Commun. Mag.*, vol. 47, no. 1, pp. 84–89, Jan. 2009.
- [9] N. Nowsheen, C. Benson, and M. Frater, "A high data-rate, software-defined underwater acoustic modem," in *OCEANS 2010 MTS/IEEE SEATTLE*, 2010, pp. 1–5.
- [10] M. S. Martins, N. Pinto, J. P. Carmo, and J. Cabral, "High data rate acoustic modem for underwater applications," in *2014 International Telecommunications Symposium (ITS)*, 2014, pp. 1–5.
- [11] M. S. Martins, N. Pinto, G. Rocha, J. Cabral, and S. Laceros Mendez, "Development of a 1 Mbps low power acoustic modem for underwater communications," in *2014 IEEE International Ultrasonics Symposium*, 2014, pp. 2482–2485.
- [12] "Cetacean Research Technology." [Online]. Available: <http://www.cetaceanresearch.com/hydrophones/c304-hydrophone/index.html>.
- [13] C. H. Sherman and J. L. Butler, *Transducers and Arrays for*

Underwater Sound. Springer Science+Business Media, LLC, 2007.

[14] D. J. Leo, *Engineering Analysis of Smart Material Systems*. John Wiley & Sons, Inc., 2007.
 [15] K. B. Wolf and G. Krotzsch, "Geometry and dynamics in refracting systems," *Eur. J. Phys.*, vol. 16, no. 1, pp. 14–20, Jan. 1995.
 [16] M. Martins, V. Correia, J. M. Cabral, S. Lanceros-Mendez,

and J. G. Rocha, "Optimization of piezoelectric ultrasound emitter transducers for underwater communications," *Sensors Actuators A Phys.*, vol. 184, pp. 141–148, Sep. 2012.
 [17] C. Erdogan, I. Myderrizi, and S. Minaei, "FPGA Implementation of BASK-BFSK-BPSK Digital Modulators [Testing Ourselves]," *IEEE Antennas Propag. Mag.*, vol. 54, no. 2, pp. 262–269, Apr. 2012.

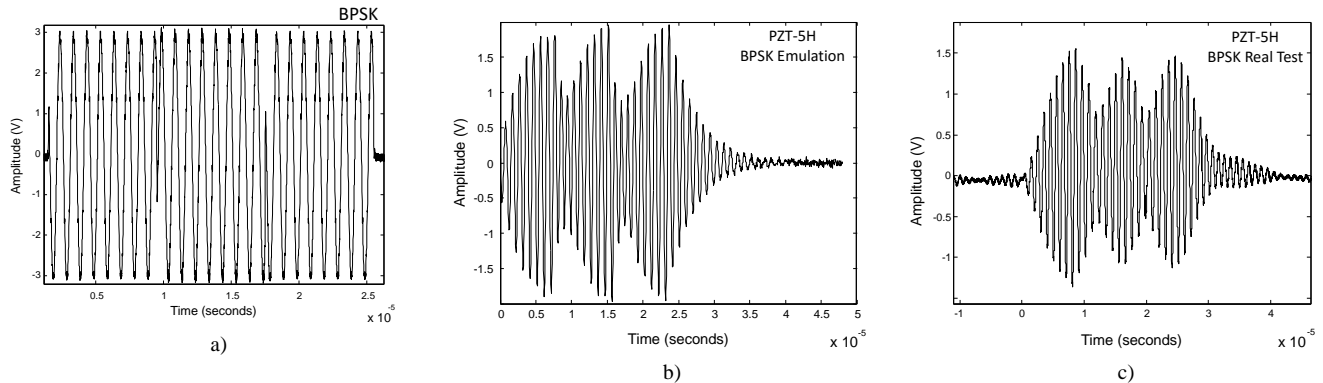


Figure 6. BPSK modulation signal (a), FPGA emulation (b) and real test signal (c).

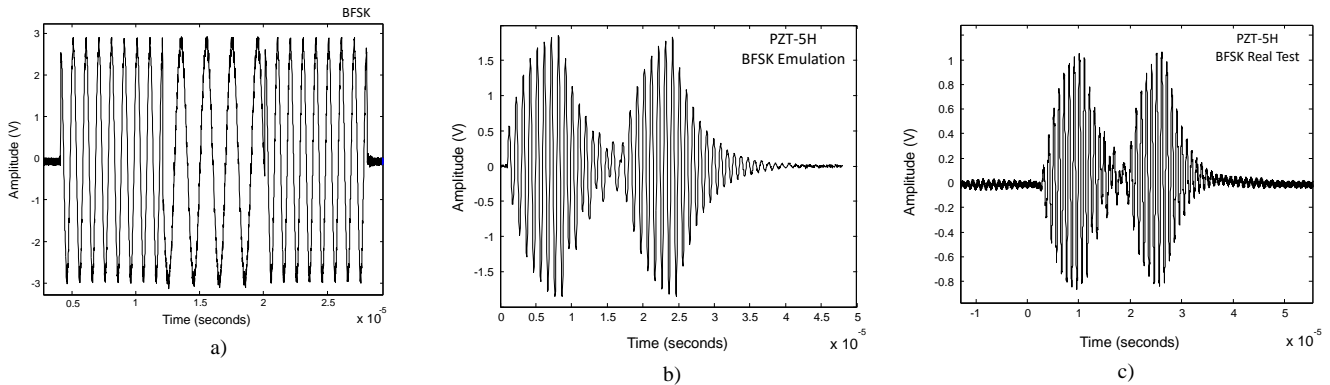


Figure 7. BFSK modulation signal (a), FPGA emulation (b) and real test signal (c).

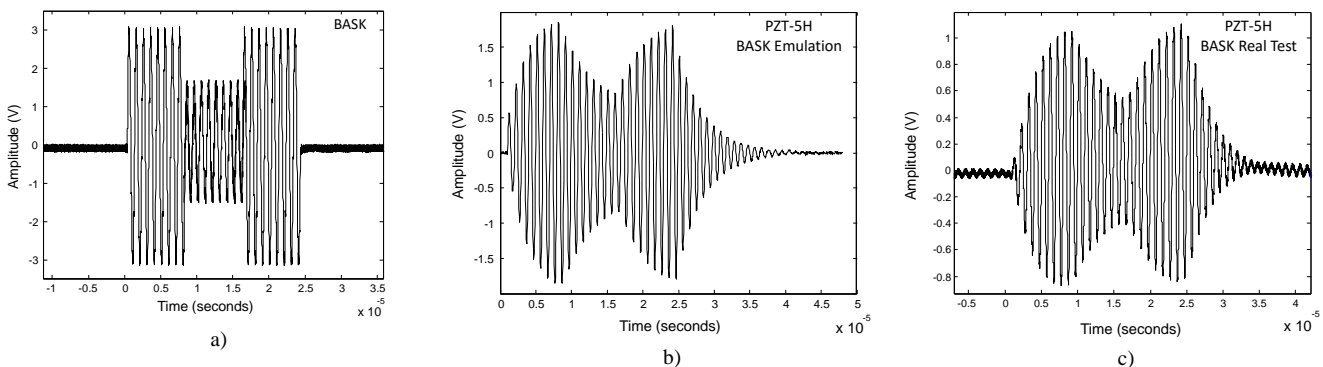


Figure 8. BASK modulation signal (a), FPGA emulation (b) and real test signal (c).